Heliyon 9 (2023) e21900

Contents lists available at ScienceDirect

Heliyon

journal homepage: www.cell.com/heliyon

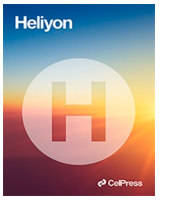

Improved photocatalytic degradation of rhodamine B by g-C_3N_4 loaded $BiVO_4$ nanocomposites

Priti Rohilla [a], Bonamali Pal [a,b], Raj Kumar Das [a,b,*]

[a] School of Chemistry and Biochemistry, Thapar Institute of Engineering & Technology, Patiala, 147004, Punjab, India
[b] TIET-Virginia Tech Center of Excellence in Emerging Materials, Thapar Institute of Engineering and Technology, Patiala, 147004, India

ARTICLE INFO

Keywords:
$BiVO_4$
Binary composite
Photocatalysis
Wastewater treatment
Emerging contaminants

ABSTRACT

Photocatalytic degradation has emerged as one of the most efficient methods to eliminate toxic dyes from wastewater. In this context, graphitic nitride (g-C_3N_4) loaded $BiVO_4$ nanocomposites (5 wt% g-CN@$BiVO_4$ and 10 wt% g-CN@$BiVO_4$) have been fabricated by the wet impregnation method, and their efficiency towards photocatalytic removal of rhodamine B have been investigated under visible light irradiation. These hybrid composites have been characterized by XRD, FESEM, HRTEM, EDS-mapping, UV-Vis DRS, DLS, XPS and BET, etc. The HRTEM images revealed that $BiVO_4$ has a decagonal shape covered by a layered nanosheet-like structure of g-C_3N_4. BET measurements suggest increasing the proportion of g-C_3N_4 results enhancement of the specific surface area. Among different photocatalysts, the 10 wt% g-C_3N_4@$BiVO_4$ hybrid possesses the best catalytic activity with 86% degradation efficiency after 60 min of reaction time. The LC-MS studies suggest that the degradation reactions follow the de-ethylation pathway. Even after five cycles, the heterostructure shows only a 14% decrease in photocatalytic activity, confirming its stability. As a result, the binary composite can be regarded as a promising catalyst for the degradation of pollutants due to its ease of preparation, high stability and superior catalytic activity.

1. Introduction

Water contamination has played a significant role in the recent increase in worldwide environmental pollution, which is primarily due to the textile industry. According to studies, between 10 and 12% of the dyes are classified as hazardous waste, with Rhodamine B being one of the contaminants [1,2]. Rhodamine B, a member of the xanthene family, is frequently employed in the textile industry due to its stability, solubility in water, and brightness [3]. Even at smaller concentrations (1 ppm), the dye has a detrimental impact on the aquatic environment [4]. The dye has a dangerous and mutagenic effect in that it harms people by affecting their brain, central nervous system, liver, and kidneys [5]. As a result, many techniques for their removal have been developed [6].

The reliable method for removing toxins from water is thought to be semiconductor-based photocatalysts. $BiVO_4$ has emerged as an excellent photocatalyst due to its narrow band gap (2.4eV), low toxicity, corrosion resistance, chemical stability, etc [7,8]. The photoactivity of bare $BiVO_4$ is not very significant due to the rapid electron-hole pair recombination rate and smaller specific surface area [9]. Therefore, combining it with other materials, such as metals and non-metals, to create composites with heterojunction structures has now emerged as a great option [10]. Such methodologies result in an improvement of the sensitivity towards visible light

* Corresponding author. School of Chemistry and Biochemistry, Thapar Institute of Engineering & Technology, Patiala, 147004, Punjab, India.
E-mail address: rkdas@thapar.edu (R.K. Das).

https://doi.org/10.1016/j.heliyon.2023.e21900
Received 26 August 2023; Received in revised form 10 October 2023; Accepted 31 October 2023
Available online 5 November 2023

and a reduction in electron-hole pair recombination. Numerous investigations have shown that composites have higher photocatalytic activity than bare $BiVO_4$ [11]. Due to the potential and fundamental physical characteristics, graphitic nitride (g-C_3N_4), a 2D layered and metal-free structured material, is currently attracting a lot of interest [12–16]. Fabrication heterojunction interface allows the effective separation of photogenerated electrons and holes. Additionally, the direction of charge transfer changes in accordance with the semiconductor's band position [17]. The development of the heterojunction structure of both semiconductors has proven to be an appropriate solution; as a result of the band positions of g-C_3N_4 and $BiVO_4$ matching, the separation of charge and recombination rate is effectively controlled and also enhances the photocatalytic activity [18]. There have not been many reports on the wet chemical methods used to create a composite of $BiVO_4$/g-C_3N_4 with varying weight ratios, whose photocatalytic performance was examined.

2. Experimental

2.1. Chemicals

All the chemicals Bismuth nitrate pentahydrate 98% [Bi $(NO_3)_3{\cdot}5H_2O$], Ammonium metavanadate 99% [NH_4VO_3], Urea 99% extra pure, Rhodamine B. [RhB], N-Methyl-2-pyrrolidone (NMP) were procured from Loba Chemie, India. The carbon black (CB) powder, polyvinylidene fluoride (PVDF), and fluorinated tin oxide (FTO) glasses (resistance <10 Ω) were purchased from Nanoshell, Sigma Aldrich, and Vritra Technologies, respectively. Ethanol (absolute) 99.9% was obtained from Changshu Hongsheng Fine Chemicals Co. Ltd. Deionized water was prepared using Milli-Q, Millipore ultrafiltration system.

2.2. Preparation of $BiVO_4$

$BiVO_4$ (denoted as BVO) was prepared by homogeneous precipitation method, in which Bi $(NO_3)_3{\cdot}5H_2O$ [6 mmol] was dispersed in a 32 mL aqueous solution of 1 M HNO_3 using ultrasonication. After that, NH_4VO_3 [6 mmol] was added to the above solution and strenuously stirred for 1 h. Subsequently, 3 g urea was added and heated the mixture at 80 °C using an oil bath for 24 h. Then yellow-colour precipitate was filtered and washed with DI water & ethanol and dried at 60 °C overnight [9].

2.3. Preparation of g-C_3N_4

In a crucible, 12 g of urea was added to 50 mL of DI water and placed in an oven at 60 °C (12 h) for recrystallization. After recrystallization, covered it properly with aluminium foil and placed in a muffle furnace for 2 h at 550 °C with a 10 °C/min rise in temperature. A light brownish-colored solid product of g-C_3N_4 was grounded as a fine powder and denoted as g-CN [19].

2.4. Preparation of g-CN loaded BVO composite

The composite was prepared by wet impregnation chemical followed by solvent evaporation method [20,21]. For the synthesis of g-C_3N_4@$BiVO_4$ composite, firstly dispersed 50 mg $BiVO_4$ in 20 mL ethanol, and the mixture was sonicated for 1 h. After 1 h, the required amount of g-C_3N_4 was added to the mixture and sonicated for another 1 h then the mixture was kept for stirring for 24 h. Now, the obtained composite was kept in an oven at 50 °C for drying. The composite is abbreviated as BCN-1 for 5 wt% loading of g-CN@BVO and BCN-2 for 10 wt% loading of g-CN@BVO.

2.5. Preparation of thin films

The films for the EIS Nyquist plot were prepared on FTO glass by drop cast method. Initially, 1 mg of PVDF and 40–60 μL NMP were mixed thoroughly to result in a uniform paste, then 1 mg CB was added to this mixture and blended further for 20 min. Subsequently, 8 mg of the active material (BVO or BCN-2) was also added and combined further to obtain a homogeneous mixture, which was drop-casted into a clean FTO. The coated FTO substrate was dried at 80 °C overnight.

2.6. Photocatalytic activity evaluation

The toxic pollutant RhB (Rhodamine B) was chosen to scrutinize the photocatalytic properties of as prepared $BiVO_4$ and its composite prepared by 5 wt% loading of g-CN@BVO (named as BCN-1) and 10 wt% loading of g-CN@BVO (named as BCN-2). In a typical experiment, 7.5 mg of the photocatalyst was added to a test tube containing 5 ml of RhB solution (0.0183 mM) at room temperature. Before the photocatalytic degradation experiment, the suspension was stirred in the dark for 30 min to attain the adsorption-desorption equilibrium. After that, the test tube was illuminated with visible light irradiation (Wipro Garnet B22-50 W LED bulb, $\lambda > 360$ nm) for monitoring degradation at fixed time intervals. By centrifugation, catalysts were separated out, and the concentration of RhB pollutant was examined in the corresponding solution using a UV-Vis spectrophotometer (Shimadzu UV-2600). The following equation was used to calculate the degradation efficiency:

$$\text{Degradation efficiency}(\%) = \frac{\boldsymbol{C_0} - \boldsymbol{C_t}}{\boldsymbol{C_0}} \times \mathbf{100}$$

where $\mathbf{C_0}$ is the initial concentration of the pollutant, $\mathbf{C_t}$ is concentration after 't' time.

2.7. Characterization technique

The crystallographic properties were recorded by X-ray diffraction (XRD) using Xpert pro-Cu-Kα (1.54 Å) at 45 kV with a diffraction angle 2θ (15°–65°). The structural morphology was investigated with field emission scanning electron microscopy (FESEM, Carl-Zeiss Sigma 500 FEG-SEM) and EDS (energy dispersive spectroscopy) for elemental composition by BRUKER and high-resolution transmission electron microscopy (HRTEM, JEOL JEM 2100 plus). The optical absorption spectra of bare BVO and its composites (BCN-1 and BCN-2) were studied with a diffuse reflectance spectrophotometer (solid state, Shimadzu UV-2600). The hydrodynamic size was recorded with a zeta potential analyzer (ZEN 3600, Malvern, U.K.). The oxidation state was confirmed by X-ray Photoelectron spectroscopy (XPS, Thermo Fischer Scientific ESCALAB Xi). The N_2 adsorption-desorption was carried out by (Quanta chrome Nova 2200e). The band gaps were determined by monitoring its diffused reflectance spectra (DRS) using UV-visible spectrophotometer (Shimadzu UV-2600). The intermediates were detected by HRMS (Waters, QTOF mass spectrometer with UPLC (XEVO G2 XS) and Ion source - Combined ESI and APCI source with positive and negative mode scans, at different time intervals, retention time 8 min). The electrochemical impedance spectroscopy (EIS) experiments were performed at a voltage of 0.7 V vs RHE in the frequency range from 1 Hz to 1000 Hz using a Biologic VSP300 potentiostat under the dark. The BVO and BCN-2 loaded FTO were used as the working electrode, Pt as the counter electrode, and the standard calomel electrode as the reference electrode in 0.5 M Na_2SO_4 (pH = 6.5). FTIR was recorded by IRTracer-100 (Fourier Transform Infrared Spectrophotometer, Shimadzu).

3. Result and discussion

3.1. XRD studies

XRD analyzed the phase structure of samples, Fig. 1a contains the XRD pattern of g-CN in which the strong intensity peak lies at the (002) plane at 27.9° and another peak at 12.7° for the (100) plane [19], and there are two extra peaks in the diffraction field of 15°–25° which could be due to the crystallographic planes in the graphitic nitride layered structure [22]. It could be seen that the bare $BiVO_4$ (Fig. 1b) was in good agreement with the monoclinic scheelite phase (ICDD PDF card number 14–0688) [9]. In Fig. 1b, the peaks indicate the presence of no phase impurity, as evidenced by the absence of any extra diffraction peak. The XRD pattern for the composites, BCN-1 and BCN-2 (Fig. 1c) is exactly similar to the bare BVO and has no corresponding peak of g-CN. Such observation is quite reasonable as g-CN has a much smaller x-ray scattering coefficient than BVO. It also confirms that upon loading of g-CN in the BVO surface, there is no significant effect on its structural integrity [23,24].

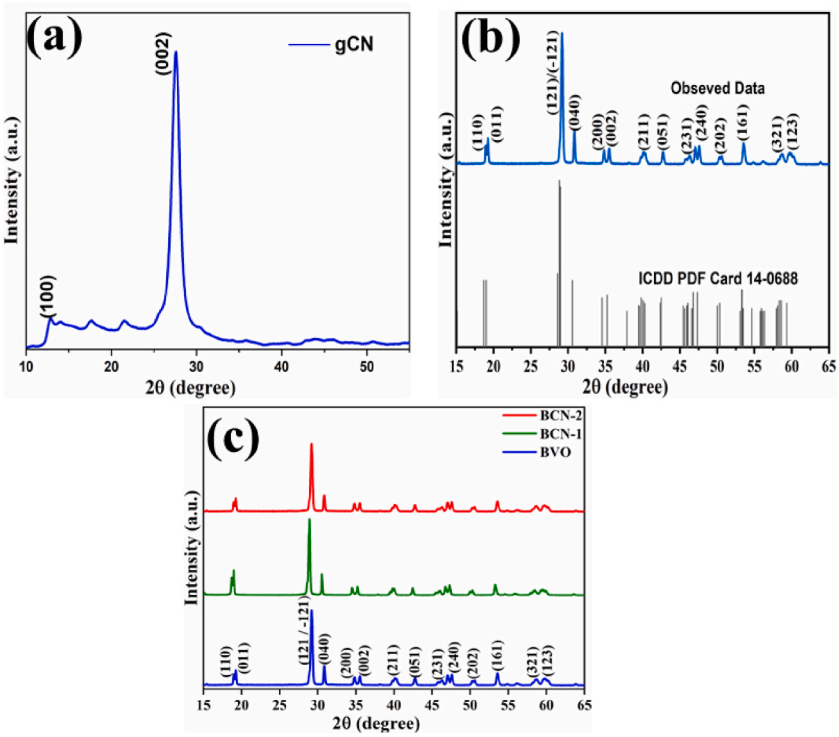

Fig. 1. XRD patterns of (a) g-CN, (b) BVO and (c) BVO, BCN-1 and BCN-2 composites.

3.2. XPS analysis

The XPS plot of g-CN doped $BiVO_4$ composite (BCN-2) is shown in Fig. 2. The survey diagram in Fig. 2a, indicates the presence of elements Bi, C, N, V and O in the composite. The peaks at 158.0eV and 163.3eV binding energy correspond to Bi ($4f_{7/2}$) and Bi ($4f_{5/2}$), respectively, validating Bi's trivalent oxidation state. Fig. 2b [25,26]. In Fig. 2c, The V $2p_{3/2}$ (515.7eV) and $2p_{1/2}$ (523.1eV) signals can be ascribed to the V^{5+} species [27,28]. As observed in Fig. 2d, the XPS spectrum of C 1s has peaks at 284.1eV and 287.4eV, which are characteristic of the C–C bond and C–N bond, respectively, in which C attached to the $–NH_2$ group and is in sp^2 state in aromatic ring [29]. Meanwhile, the allocation of the peak at 397.8eV in Fig. 2e was assigned to N-atom in triazine rings (C=N–C) having sp^2 hybridization and a less intense peak at a high binding energy of 399.3eV consisting of centered/bridged sp^2 N-atom which is further attached to C- atom like $N-(C)_3$ [30,31]. Fig. 2f represents the XPS spectrum of O 1s in which the peaks were deconvoluted into two peaks with binding energy at 528.8eV and 531.8eV, which are characteristic of the lattice oxygen and surface-absorbed water, respectively [30,32]. The absence of any other elements confirms the chemical purity of the g-CN/$BiVO_4$ composite.

3.3. Optical property

To determine the optical bandgap, the UV-Vis diffuse reflectance spectrum of the as-prepared photocatalysts was recorded. As shown in Fig. S1a, the bare $BiVO_4$ shows the absorption edge at 516 nm, which is in good agreement with the reported result [9]. The bandgap energy of the bare BiVO4 photocatalyst is determined with the help of a Tauc plot, as shown in Fig. S1b. With the increase in the loading of g-CN [22], the bandgap gradually decreases from 2.37eV ($BiVO_4$) to 2.30eV (BCN-2).

3.4. EIS measurements

In order to investigate the change transfer characteristics, the electrochemical impedance spectroscopic (EIS) measurements were carried out for BVO and the BCN-2 composites in the dark. It has been noticed that the Nyquist plot of the BCN-2 composite has smaller radii than the pristine BVO (Fig. S2). Such observation suggests that the BCN-2 composite has a lower charge transfer resistance than the original BVO.

3.5. Morphology

FE-SEM images were recorded to investigate the morphology of the pure $BiVO_4$ and its composite with g-C_3N_4 by the loading amount (10 wt%) of g-CN@$BiVO_4$, named BCN-2, shown in Fig. 3. It was noticed that the morphology of bare $BiVO_4$ sample exhibit

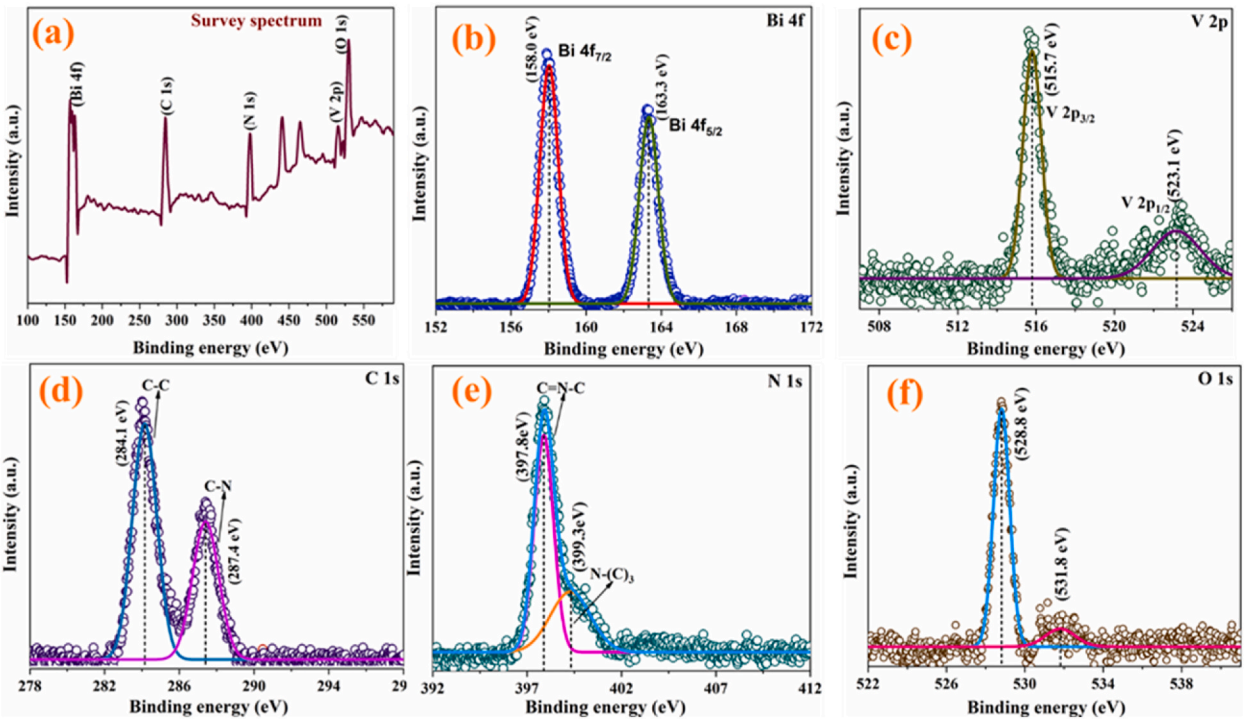

Fig. 2. XPS spectra of BCN-2 composite showing (a) survey spectrum and deconvoluted peaks of (b) Bi 4f (c) V 2p (d) C 1s (e) N 1s (f) O 1s respectively.

decagonal shape in Fig. 3a-b where the well-formed crystal displayed sharp edges and smooth surface [9]. The average particle size of BVO was found to be 225 nm, shown in Fig. S3. The FE-SEM image of the BCN-2 composite demonstrates the presence of both deposition of $BiVO_4$ crystals and CN layers (Fig. 3c–e) [19], thereby confirming the formation of the composite. In HRTEM, the dark grey-colored portions represent the BVO, whereas the light grey areas correspond to the g-CN sheets. The HRTEM images clearly show the deposition of g-CN sheets over the $BiVO_4$, particles. Moreover, the lattice fringes of 0.49 nm in Fig. 4c were assigned to the (110) plane of $BiVO_4$ [18] which showed that its crystallinity is retained in the composite. The EDS mapping of the prepared samples was analyzed to determine the elemental composition present in the samples. The EDS mapping shows the particular region over which the distribution of the different elements was present, as shown in Fig. S4 and Fig. 5 for $BiVO_4$ and BCN-2 composite (which contains C, N, Bi, V, O) respectively.

The hydrodynamic particle size of the photocatalyst can be recorded with the Dynamic light scattering technique. It was found that the hydrodynamic sizes of the particles are 612 nm, 639 nm, and 684 nm, for $BiVO_4$, BCN-1, and BCN-2, respectively (Fig. S5). The increase in the size is due to the loading of layered g-CN sheets on $BiVO_4$.

3.6. N_2 adsorption-desorption analysis

Using BET analysis, the surface properties of the as-prepared material were analyzed (Fig. 6). The prepared samples consisted of type-III adsorption-desorption isotherm having an H3 hysteresis loop [33]. The surface area of $BiVO_4$ is 6.7 m^2/g and the BCN-2 composite is 13.4 m^2/g in Fig. 6b, respectively. The loading of graphitic nitride on $BiVO_4$ enhances the number of active sites, thereby increasing the specific surface area. So, the composite can act as a superior photocatalyst due to its higher surface area [34].

3.7. Photocatalytic degradation

RhB was adopted as the model pollutant for the photodegradation experiment to evaluate the photocatalytic activity of synthesized composite in the presence of visible light [35] (Fig. 7). The initial concentration of RhB was 0.0183 mM. Before illuminating the light, the reaction mixture was stirred for 30 min in the dark to attain adsorption-desorption equilibrium. After 60 min, the $BiVO_4$ was given only ~19% degradation efficiency. The degradation efficeincies for BCN-1 and and BCN-2 composites are ~63% and ~86%, respectively, in 60 min.

To evaluate the rate constant, the following equation [35].

$$\ln\left(\frac{C}{C_0}\right) = -kt$$

was followed and Table S1 shows the rate constant values, Fig. 7d shows the bar plot of rate constant values of different synthesized samples.

The kinetic study of bare BVO, g-CN and BCN-1 and BCN-2 composite is shown in (Fig. S6). It has been concluded that the BCN-2 composite displayed the maximum degradation efficiency in visible light.

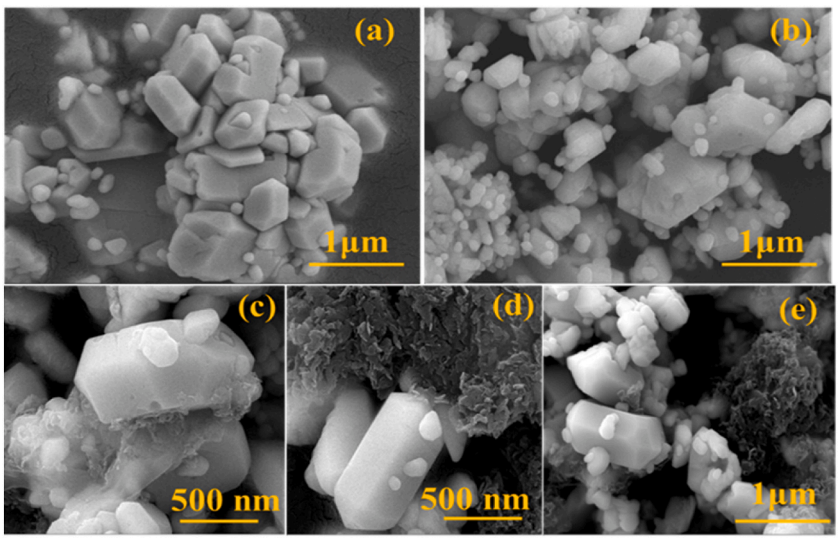

Fig. 3. FE-SEM images of BVO (a and b) and BCN-2 composite (c, d and e).

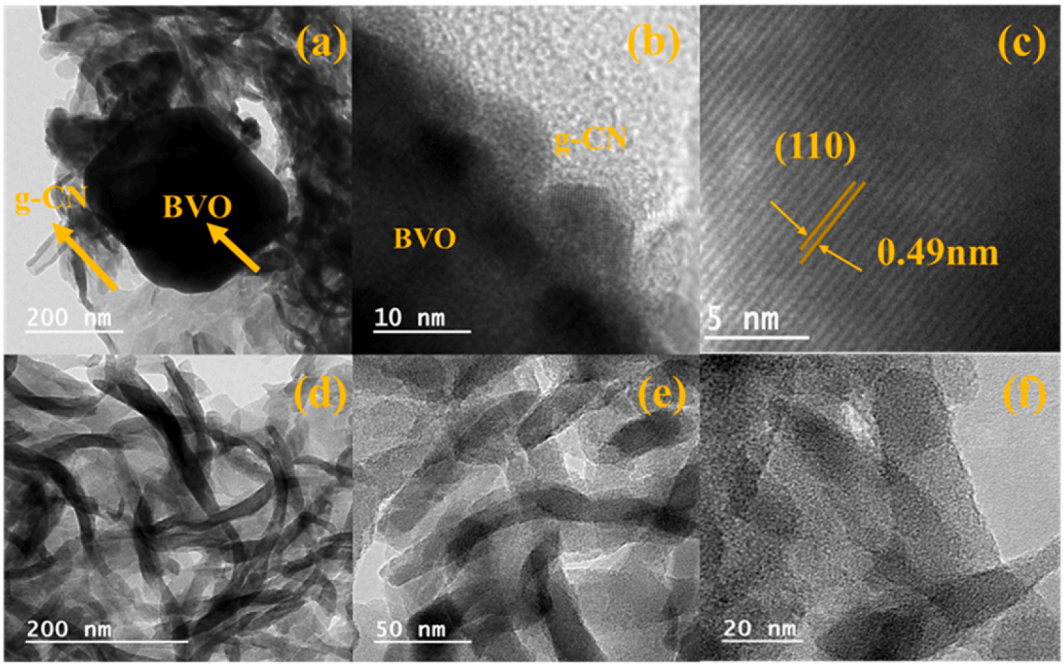

Fig. 4. HRTEM images of BCN-2 (a and b), lattice fringes (c) and g-CN (d, e, f).

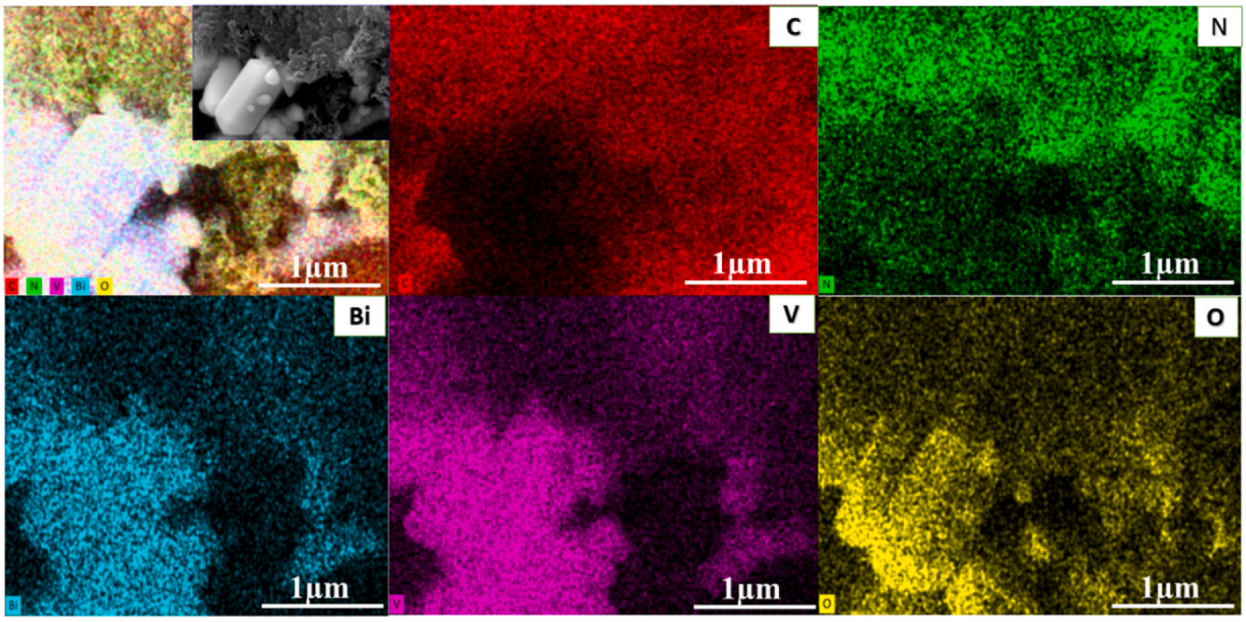

Fig. 5. Elemental dot mapping of BCN-2 composite, showing the presence of elements Bi, V, O, C and N.

3.8. Mechanistic studies

3.8.1. Mechanism

The proposed photocatalytic mechanism is based on the generation of electron-hole pairs by excitation through a band gap (Fig. 8), a type-II heterojunction structure [38–41]in which the electrons (e^-) that are excited in CB of g-CN will transfer to the CB of BVO and corresponding holes (h^+) in VB of BVO will migrate to the VB of g-CN which reduces the electron-hole pair recombination. The hydroxyl radicals (OH) and superoxide anions (O_2) are produced by redox interactions between the electrons and holes and the water molecules and molecular oxygen, respectively. These reactive species photodegrade the RhB pollutant.

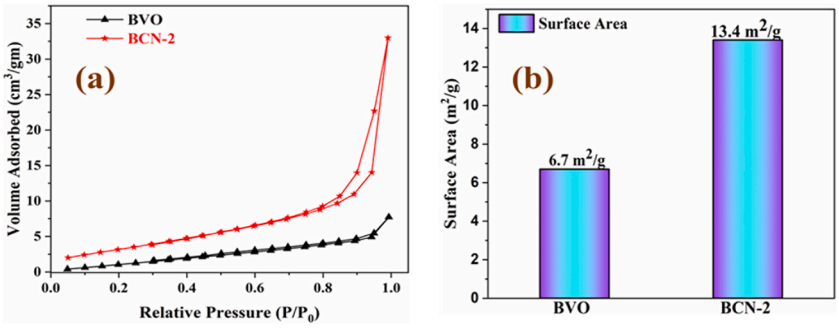

Fig. 6. N_2 adsorption-desorption isotherm of (a) $BiVO_4$ and BCN-2 composite respectively, (b) Surface area of $BiVO_4$ and BCN-2 respectively.

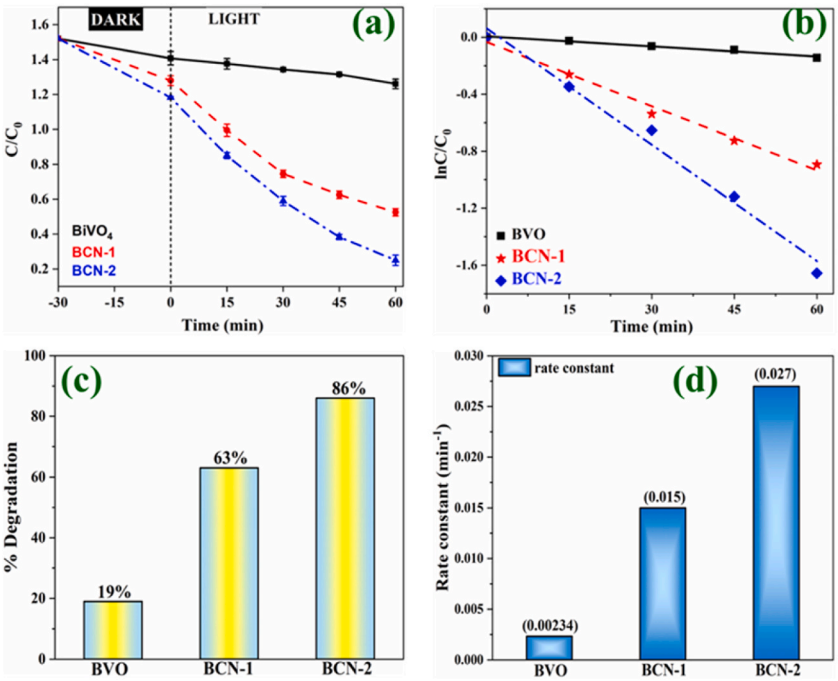

Fig. 7. Photocatalytic degradation of RhB with time (a) and showing trends with ln C/C_0 and at different time intervals of bare BVO, BCN-1 and BCN-2 composites respectively (b), (c) represents the bar graph of RhB degradation efficiency and (d) showing the bar graph of rate constant values of BVO, BCN-1 and BCN-2 respectively.

The band edge potential energies of BVO and g-C_3N_4 were calculated by the following equation to support the proposed mechanism [36].

$$E_{VB} = X\text{-}E_e + 0.5E_g$$

$$E_{CB} = E_{VB} - E_g$$

where, E_{VB} = Valence band potential

E_{CB} = Conduction band potential
X = Electronegativity of semiconductor (geometric mean of electronegativities of its constituent elements)
E_e = Energy of free electron
E_g = Band gap energy

The E_{VB} value for $BiVO_4$ and g-C_3N_4 is +2.85eV and +1.64eV respectively and E_{CB} is +0.48eV for $BiVO_4$ and −1.29eV for g-C_3N_4. There is a positive electrode potential of both the VB as well as CB for $BiVO_4$ as compared with the VB and CB of g-C_3N_4 [37].

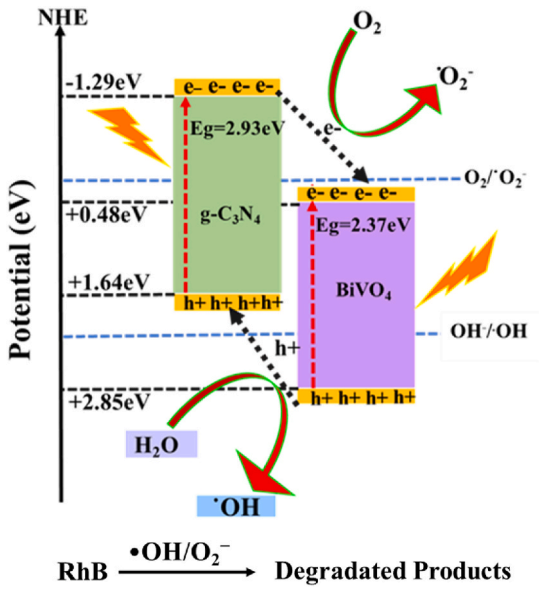

Fig. 8. A plausible mechanism for the photocatalytic degradation of RhB by using BCN-2 composite (10 wt% g-C_3N_4 @$BiVO_4$).

3.8.2. *Scavengers effect*

To evaluate the role of reactive species, a number of control studies were conducted with EDTA, Argon gas purging, iPA, and NH_4SCN (Fig. 9). It was observed that the degradation efficiency of the reaction mixture is decreased by the addition of EDTA, iPA, and NH_4SCN from 86% to 37%, 76%, and 62.2%, respectively. They function as hole scavengers which effectively prevent the production of hydroxyl radicals during the oxidation of water molecules by holes.

Additionally, the photocatalytic degradation efficiency drops to 71.5% after the purging of Ar gas. This is due to the elimination of oxygen from the reaction mixture caused by the argon purging, which lowers the feasibility of superoxide radical production. According to this result, photocatalytic oxidation activities are likely promoted by both superoxide anions and hydroxide radicals [42].

3.8.3. *HRMS studies*

In order to identify the intermediates, HPLC-MS studies were carried out (Scheme 1) and in (Fig. S7). The signal at *m/z* 443 is characteristic of the parent RhB molecule. Apart from this the MS spectra also give prominent signals at *m/z* 415, 387, 359 and 331 corresponding to different de-ethylated intermediates [43,44]. Such observation suggests that the degradation process proceeds through de-ethylation pathway [44–46].

3.9. *Recyclability of photocatalyst*

In order to investigate the stability of the BCN-2 photocatalyst, recyclability studies were performed (Fig. 10). The photocatalyst was recovered from the reaction mixture after the photodegradation process and reused in the following reaction under identical conditions. The recyclability of the photocatalyst is inspected with the help of 5 runs in the degradation of RhB. The degradation efficiencies were found to be 87%, 86%, 81%, 78% and 74% from the first to fifth cycle. Interestingly, there is only a 13% decrease in photocatalytic efficiency than the initial cycle, which can be due to the loss of amount during washing/centrifugation and drying [47].

3.10. *Stability of photocatalyst*

In order to confirm the stability of the photocatalyst further, FTIR, XRD, and SEM of the BCN-2 composite before and after the reaction have been performed (Figs. 11 and 12). It has been observed that the FTIR spectra (Fig. 11) and XRD patterns (Fig. 12a) remain practically similar before and after the photocatalytic reactions. The SEM images (Fig. 12b) reveal that the morphology of BCN-2 remains similar before and after the reactions. All these observations confirm the stability of the photocatalyst and rules out any possibility of dissociation or leaching during catalytic reactions.

4. Conclusion

In conclusion, this report involves the design of g-C_3N_4/$BiVO_4$ nanocomposites and the evaluation of their photocatalytic degradation activity towards the removal of RhB from wastewater under visible light radiation. The controlled experiments revealed that both hydroxide radicals and superoxide ions are the main reactive species in the photodegradation process. The HPLC MS studies reveal that the photocatalytic reaction proceeds via de-ethylation mechanism. Moreover, the recyclability experiments confirmed the

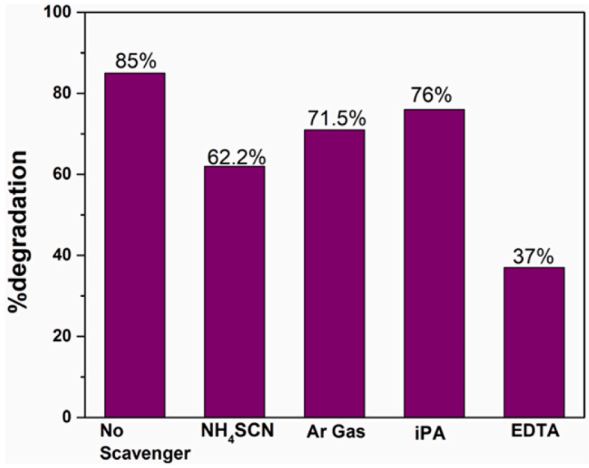

Fig. 9. Plot showing the variation of photocatalytic degradation of 10 wt% g-CN@BVO (BCN-2 composite) after the purging of Ar and upon the addition of NH_4SCN, iPA and EDTA.

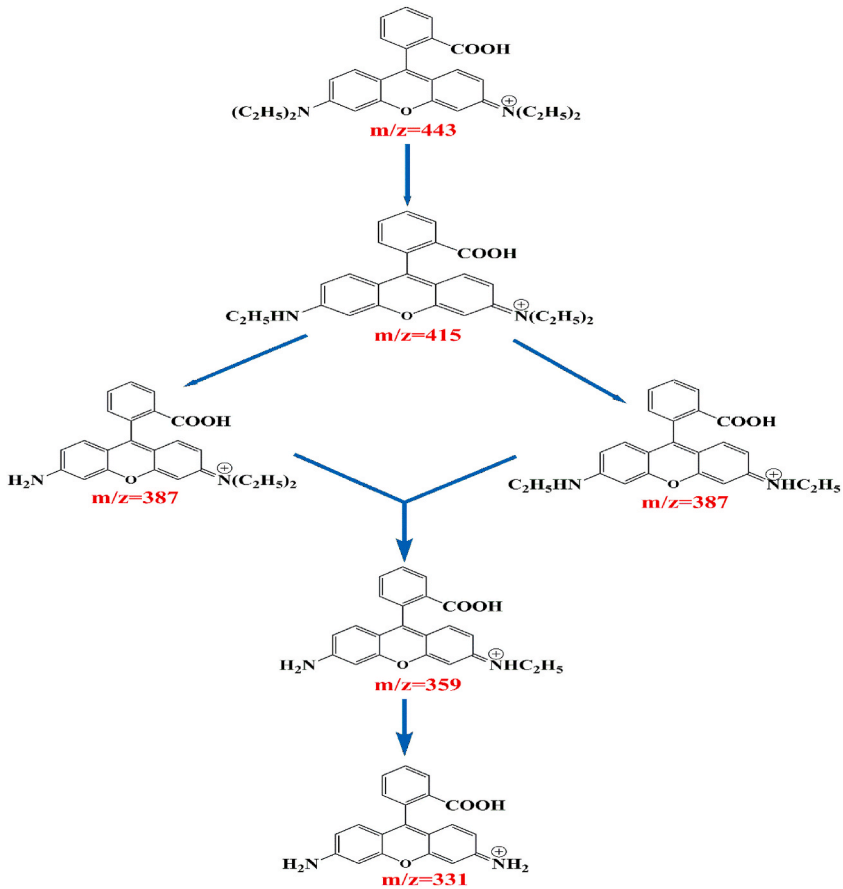

Scheme 1. A probable mechanism for the photodegradation of Rhodamine B dye using BCN-2 catalyst.

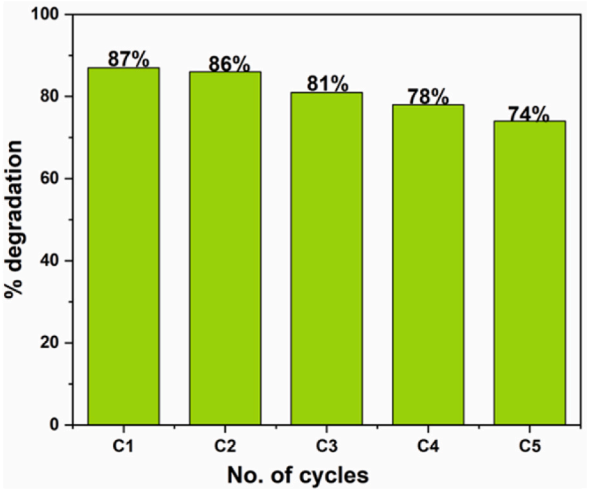

Fig. 10. Recyclability of the BCN-2 composite for the degradation of RhB using a visible light source for five successive runs.

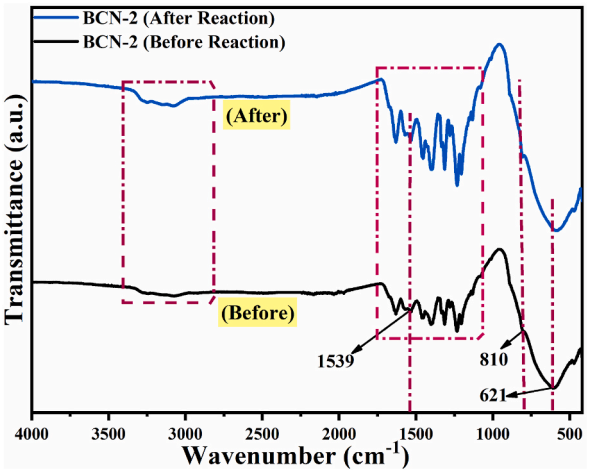

Fig. 11. FTIR spectra of BCN-2 composite before and after the photocatalytic reaction.

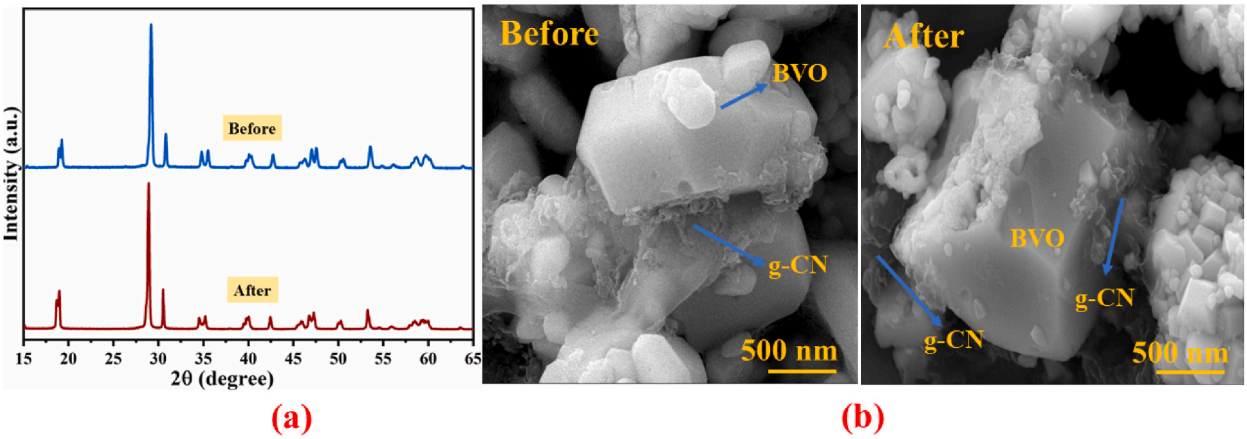

Fig. 12. (a) XRD patterns and (b) FESEM images of BCN-2 heterostructure before and after the photocatalytic reaction.

stability of the photocatalysts. Hence, the current report will be quite helpful in designing new-generation photocatalysts for wastewater treatment.

Data availability

The data will be available on request.

CRediT authorship contribution statement

Priti Rohilla: Conceptualization, Data curation, Formal analysis, Investigation, Methodology, Validation, Visualization, Writing – original draft, Writing – review & editing. **Bonamali Pal:** Investigation, Resources, Supervision, Writing – review & editing. **Raj Kumar Das:** Conceptualization, Funding acquisition, Methodology, Resources, Supervision, Validation, Writing – review & editing, Formal analysis.

Declaration of competing interest

The authors declare that they have no known competing financial interests or personal relationships that could have appeared to influence the work reported in this paper.

Acknowledgements

The authors are thankful to SPMS, TIET for XRD, FESEM and EDS analysis. SPRINT Testing Solution- Mumbai for HRTEM, XPS and BET analysis. We are also grateful to DST-FIST (Grant number: SR/FST/CS-II/2018/69) for the HRMS facility, TIET-Patiala. The authors are also thankful to Dr. O.P. Pandey and Dr. Piyush Sharma for electrochemical measurements. We are also grateful to Dr. Soumen Basu for his help in ICDD PDF card drawing. The authors are also thankful to the TIET-VT Center of Excellence for Emerging Material (CEEMS) for funding and FTIR measurements.

Abbreviations

BVO	BiVO4
g-CN	g-C3N4
BCN-1	5 wt% g-C3N4@BiVO4
BCN-2	10 wt% g-C3N4@BiVO4
RhB	Rhodamine B
VB	Valence Band
CB	Conduction Band
DI	Distilled water
PVDF	Polyvinylidene fluoride
CB (in EIS experiment)	Carbon black
NMP	N-Methyl-2-pyrrolidone

Appendix A. Supplementary data

Supplementary data to this article can be found online at https://doi.org/10.1016/j.heliyon.2023.e21900.

References

[1] A. Rafiq, M. Ikram, S. Ali, F. Niaz, M. Khan, Q. Khan, M. Maqbool, Photocatalytic degradation of dyes using semiconductor photocatalysts to clean industrial water pollution, J. Ind. Eng. Chem. 97 (2021) 111–128, https://doi.org/10.1016/j.jiec.2021.02.017.

[2] S. Chen, J. Zhang, C. Zhang, Q. Yue, Y. Li, C. Li, Equilibrium and kinetic studies of methyl orange and methyl violet adsorption on activated carbon derived from Phragmites australis, Desalination 252 (2010) 149–156, https://doi.org/10.1016/j.desal.2009.10.010.

[3] C. Hu, A.T. Le, S.Y. Pung, L. Stevens, N. Neate, X. Hou, D. Grant, F. Xu, Efficient dye-removal via Ni-decorated graphene oxide-carbon nanotube nanocomposites, Mater. Chem. Phys. 260 (2021), 124117, https://doi.org/10.1016/j.matchemphys.2020.124117.

[4] N. Daneshvar, D. Salari, A.R. Khataee, Photocatalytic degradation of azo dye acid red 14 in water: Investigation of the effect of operational parameters, J. Photochem. Photobiol. Chem. 157 (2003) 111–116, https://doi.org/10.1016/S1010-6030(03)00015-7.

[5] Z. Ajji, A.M. Ali, Adsorption of methyl violet and brilliant blue onto poly(vinyl alcohol) membranes grafted with N-vinyl imidazole/acrylic acid, Nucl. Instrum. Methods Phys. Res. B 265 (2007) 362–365, https://doi.org/10.1016/j.nimb.2007.09.004.

[6] T.O. Ajiboye, O.A. Oyewo, D.C. Onwudiwe, Adsorption and photocatalytic removal of Rhodamine B from wastewater using carbon-based materials, FlatChem 29 (2021), 100277, https://doi.org/10.1016/j.flatc.2021.100277.

[7] X. Lin, H. Li, L. Yu, H. Zhao, Y. Yan, C. Liu, H. Zhai, Efficient removal rhodamine B over hydrothermally synthesized, Mater. Res. Bull. 48 (2013) 4424–4429, https://doi.org/10.1016/j.materresbull.2013.06.075.

[8] N.G. Deshpande, C.H. Ahn, R.R. Koli, A.S. Jamadar, D.S. Kim, Y.B. Kim, S.H. Jung, Applied Surface Science Controlled nanostructured morphology of BiVO 4 photoanodes for e ffi cient on-demand catalysis in solar water-splitting and sustainable water-treatment, Appl. Surf. Sci. 514 (2020), 146075, https://doi.org/10.1016/j.apsusc.2020.146075.

[9] F. Chen, Q. Yang, X. Li, G. Zeng, D. Wang, C. Niu, J. Zhao, H. An, T. Xie, Y. Deng, Hierarchical assembly of graphene-bridged Ag3PO4/Ag/BiVO4 (040) Z-scheme photocatalyst: an efficient, sustainable and heterogeneous catalyst with enhanced visible-light photoactivity towards tetracycline degradation under visible light irradiation, Appl. Catal., B 200 (2017) 330–342, https://doi.org/10.1016/j.apcatb.2016.07.021.

[10] Y. Wang, K. Ding, R. Xu, D. Yu, W. Wang, P. Gao, B. Liu, Fabrication of BiVO4/BiPO4/GO composite photocatalytic material for the visible light-driven degradation, J. Clean. Prod. 247 (2020), https://doi.org/10.1016/j.jclepro.2019.119108.

[11] Y. Wang, D. Yu, W. Wang, P. Gao, L. Zhang, S. Zhong, B. Liu, The controllable synthesis of novel heterojunction CoO/BiVO4 composite catalysts for enhancing visible-light photocatalytic property, Colloids Surf. A Physicochem. Eng. Asp. 578 (2019), 123608, https://doi.org/10.1016/j.colsurfa.2019.123608.

[12] H. Tian, M. Liu, W. Zheng, Constructing 2D graphitic carbon nitride nanosheets/layered MoS2/graphene ternary nanojunction with enhanced photocatalytic activity, Appl. Catal., B 225 (2018) 468–476, https://doi.org/10.1016/j.apcatb.2017.12.019.

[13] W. Zhang, Y. Ma, X. Zhu, S. Liu, T. An, J. Bao, X. Hu, H. Tian, Fabrication of Ag decorated g-C3N4/LaFeO3 Z-scheme heterojunction as highly efficient visible-light photocatalyst for degradation of methylene blue and tetracycline hydrochloride, J. Alloys Compd. 864 (2021), https://doi.org/10.1016/j.jallcom.2021.158914.

[14] J. Bao, X. Jiang, L. Huang, W. Quan, C. Zhang, Y. Wang, H. Wang, Y. Zeng, W. Zhang, Y. Ma, S. Yu, X. Hu, H. Tian, Molybdenum disulfide loading on a Z-scheme graphitic carbon nitride and lanthanum nickelate heterojunction for enhanced photocatalysis: interfacial charge transfer and mechanistic insights, J. Colloid Interface Sci. 611 (2022) 684–694, https://doi.org/10.1016/j.jcis.2021.12.106.

[15] N. Fajrina, M. Tahir, Monolithic Ag-Mt dispersed Z-scheme pCN-TiO2 heterojunction for dynamic photocatalytic H2 evolution using liquid and gas phase photoreactors, Int. J. Hydrogen Energy 45 (2020) 4355–4375, https://doi.org/10.1016/j.ijhydene.2019.11.194.

[16] S.S. Lam, V.H. Nguyen, M.T. Nguyen Dinh, D.Q. Khieu, D.D. La, H.T. Nguyen, D.V.N. Vo, C. Xia, R.S. Varma, M. Shokouhimehr, C.C. Nguyen, Q. Van Le, W. Peng, Mainstream avenues for boosting graphitic carbon nitride efficiency: towards enhanced solar light-driven photocatalytic hydrogen production and environmental remediation, J Mater Chem A Mater 8 (2020) 10571–10603, https://doi.org/10.1039/d0ta02582h.

[17] X. Guo, J. Duan, W. Wang, Z. Zhang, Modi fi ed graphitic carbon nitride as the photocatalyst for wastewater treatment under visible light irradiation, Fuel 280 (2020), 118544, https://doi.org/10.1016/j.fuel.2020.118544.

[18] J. Zhao, J. Yan, H. Jia, S. Zhong, X. Zhang, L. Xu, Journal of Molecular Catalysis A : chemical BiVO 4/g-C 3 N 4 composite visible-light photocatalyst for effective elimination of aqueous organic pollutants, J. Mol. Catal. Chem. 424 (2016) 162–170, https://doi.org/10.1016/j.molcata.2016.08.025.

[19] D. Monga, D. Ilager, N.P. Shetti, S. Basu, T.M. Aminabhavi, 2D/2d heterojunction of MoS2/g-C3N4 nanoflowers for enhanced visible-light-driven photocatalytic and electrochemical degradation of organic pollutants, J. Environ. Manag. 274 (2020), 111208, https://doi.org/10.1016/j.jenvman.2020.111208.

[20] J. Singh, P. Kumari, S. Basu, Degradation of toxic industrial dyes using SnO2/g-C3N4 nanocomposites: role of mass ratio on photocatalytic activity, J. Photochem. Photobiol. Chem. 371 (2019) 136–143, https://doi.org/10.1016/j.jphotochem.2018.11.014.

[21] P. Kumari, B. Pal, R.K. Das, Superior adsorptive removal of eco-toxic drug diclofenac sodium by Zn–Al LDH-xBi2O3 layer double hydroxide composites, Appl. Clay Sci. 208 (2021), 106119, https://doi.org/10.1016/j.clay.2021.106119.

[22] M.I. Chebanenko, N.V. Zakharova, A.A. Lobinsky, V.I. Popkov, Ultrasonic-assisted exfoliation of graphitic carbon nitride and its electrocatalytic performance in process of ethanol, Reforming 53 (2019) 2072–2077, https://doi.org/10.1134/S106378261912008X.

[23] S. Dong, G.J. Lee, R. Zhou, J.J. Wu, Separation and Puri fi cation Technology Synthesis of g-C 3 N 4/BiVO 4 heterojunction composites for photocatalytic degradation of nonylphenol ethoxylate, Sep. Purif. Technol. 250 (2020), 117202, https://doi.org/10.1016/j.seppur.2020.117202.

[24] M. Zhang, Facile fabrication of BiVO 4/g-C 3 N 4 photocatalysts and its photocatalytic activity under visible light irradiation, J. Mater. Sci. Mater. Electron. 31 (2020) 1335–1342, https://doi.org/10.1007/s10854-019-02647-5.

[25] M. Han, J. Jia, The interlace of Bi2S3 nanowires with TiO2 nanorods: an effective strategy for high photoelectrochemical performance, J. Colloid Interface Sci. 481 (2016) 91–99, https://doi.org/10.1016/j.jcis.2016.07.045.

[26] M. Han, H. Guo, B. Li, J. Jia, W. Wang, Controllable coverage of Bi2S3 quantum dots on one-dimensional TiO2 nanorod arrays by pulsed laser deposition technique for high photoelectrochemical properties, New J. Chem. 41 (2017) 4820–4827, https://doi.org/10.1039/c7nj00213k.

[27] X. Lin, C. Liu, J. Wang, S. Yang, J. Shi, Y. Hong, Graphitic carbon nitride quantum dots and nitrogen-doped carbon quantum dots co-decorated with BiVO4 microspheres: a ternary heterostructure photocatalyst for water purification, Sep. Purif. Technol. 226 (2019) 117–127, https://doi.org/10.1016/j.seppur.2019.05.093.

[28] S.S. Kekade, P.V. Gaikwad, S.A. Raut, R.J. Choudhary, V.L. Mathe, D. Phase, A. Kshirsagar, S.I. Patil, Electronic structure of visible light-driven photocatalyst δ-Bi11VO19 nanoparticles synthesized by thermal plasma, ACS Omega 3 (2018) 5853–5864, https://doi.org/10.1021/acsomega.8b00564.

[29] X. Zhang, Q. Wu, Z. Du, Y. Zheng, Q. Li, Green synthesis of g-C 3 N 4 -Pt catalyst and application to photocatalytic hydrogen evolution from water splitting, Fullerenes, Nanotub. Carbon Nanostruct. 26 (2018) 688–695, https://doi.org/10.1080/1536383X.2018.1469006.

[30] N.A. Mohamed, J. Safaei, A.F. Ismail, M.F. Mohamad Noh, N.A. Arzaee, N.N. Mansor, M.A. Ibrahim, N.A. Ludin, J.S. Sagu, M.A. Mat Teridi, Fabrication of exfoliated graphitic carbon nitride, (g-C3N4) thin film by methanolic dispersion, J. Alloys Compd. 818 (2020), 152916, https://doi.org/10.1016/j.jallcom.2019.152916.

[31] Y.P. Zhu, T.Z. Ren, Z.Y. Yuan, Mesoporous phosphorus-doped g-C3N4 nanostructured flowers with superior photocatalytic hydrogen evolution performance, ACS Appl. Mater. Interfaces 7 (2015) 16850–16856, https://doi.org/10.1021/acsami.5b04947.

[32] W. Ali, H. Ullah, A. Zada, W. Muhammad, S. Ali, S. Shaheen, M.K. Alamgir, M.Z. Ansar, Z.U. Khan, H. Bilal, P.S. Yap, Synthesis of TiO2 modified self-assembled honeycomb ZnO/SnO2 nanocomposites for exceptional photocatalytic degradation of 2,4-dichlorophenol and bisphenol A, Sci. Total Environ. 746 (2020), 141291, https://doi.org/10.1016/j.scitotenv.2020.141291.

[33] A. Kundu, S. Sharma, S. Basu, Journal of Physics and Chemistry of Solids Modulated BiOCl nanoplates with porous g-C 3 N 4 nanosheets for photocatalytic degradation of color/colorless pollutants in natural sunlight, J. Phys. Chem. Solid. 154 (2021), 110064, https://doi.org/10.1016/j.jpcs.2021.110064.

[34] L. Li, M. Mao, X. She, J. Yi, M. He, L. Pan, Z. Chen, H. Xu, H. Li, Direct Z-scheme photocatalyst for efficient water pollutant degradation: a case study of 2D g-C3N4/BiVO4, Mater. Chem. Phys. 241 (2020), https://doi.org/10.1016/j.matchemphys.2019.122308.

[35] A. Nagar, S. Basu, Environmental Technology & Innovation Ternary g-C 3 N 4/Ag/BiVO 4 nanocomposite : fabrication and implementation to remove organic pollutants, Environ. Technol. Innov. 23 (2021), 101646, https://doi.org/10.1016/j.eti.2021.101646.

[36] N. Tian, H. Huang, Y. He, Y. Guo, T. Zhang, Y. Zhang, Mediator-free Direct Z-Scheme Photocatalytic System: BiVO4/g-C3n4 Organic–Inorganic Hybrid Photocatalyst with Highly Efficient Visible-Light-Induced Photocatalytic Activity, 2015, pp. 4297–4307, https://doi.org/10.1039/c4dt03905j.

[37] Y. Ji, J. Cao, L. Jiang, Y. Zhang, Z. Yi, G – C 3 N 4/BiVO 4 composites with enhanced and stable visible light photocatalytic activity, J. Alloys Compd. 590 (2014) 9–14, https://doi.org/10.1016/j.jallcom.2013.12.050.

[38] T. Jiang, F. Nan, J. Zhou, F. Zheng, Y. Weng, T.Y. Cai, S. Ju, B. Xu, L. Fang, Enhanced photocatalytic and photoelectrochemical performance of g-C3N4/BiVO4 heterojunction: a combined experimental and theoretical study, AIP Adv. 9 (2019), https://doi.org/10.1063/1.5090410.

[39] N. Tian, H. Huang, Y. He, Y. Guo, T. Zhang, Y. Zhang, Mediator-free Direct Z-Scheme Photocatalytic System: BiVO4/g-C3n4 Organic–Inorganic Hybrid Photocatalyst with Highly Efficient Visible-Light-Induced Photocatalytic Activity, 2015, pp. 4297–4307, https://doi.org/10.1039/c4dt03905j.

[40] Y. Ji, J. Cao, L. Jiang, Y. Zhang, Z. Yi, G – C 3 N 4/BiVO 4 composites with enhanced and stable visible light photocatalytic activity, J. Alloys Compd. 590 (2014) 9–14, https://doi.org/10.1016/j.jallcom.2013.12.050.

[41] K. Zhong, J. Feng, H. Gao, Y. Zhang, K. Lai, Fabrication of BiVO 4 @g-C 3 N 4 (100) heterojunction with enhanced photocatalytic visible-light-driven activity, J. Solid State Chem. 274 (2019) 142–151, https://doi.org/10.1016/j.jssc.2019.03.022.

[42] M. Chahkandi, M. Zargazi, New Water Based EPD Thin BiVO4 Film: Effective Photocatalytic Degradation of Amoxicillin Antibiotic, Elsevier B.V., 2020, https://doi.org/10.1016/j.jhazmat.2019.121850.

[43] K. Yu, S. Yang, H. He, C. Sun, C. Gu, Y. Ju, Visible light-driven photocatalytic degradation of rhodamine B over NaBiO3: pathways and mechanism, J. Phys. Chem. A 113 (2009) 10024–10032, https://doi.org/10.1021/jp905173e.
[44] G. Sharma, D.D. Dionysiou, S. Sharma, A. Kumar, A.H. Al-Muhtaseb, M. Naushad, F.J. Stadler, Highly efficient Sr/Ce/activated carbon bimetallic nanocomposite for photoinduced degradation of rhodamine B, Catal. Today 335 (2019) 437–451, https://doi.org/10.1016/j.cattod.2019.03.063.
[45] T.S. Natarajan, M. Thomas, K. Natarajan, H.C. Bajaj, R.J. Tayade, Study on UV-LED/TiO2 process for degradation of Rhodamine B dye, Chem. Eng. J. 169 (2011) 126–134, https://doi.org/10.1016/j.cej.2011.02.066.
[46] Z. He, S. Yang, Y. Ju, C. Sun, Microwave photocatalytic degradation of Rhodamine B using TiO2 supported on activated carbon: mechanism implication, J. Environ. Sci. 21 (2009) 268–272, https://doi.org/10.1016/S1001-0742(08)62262-7.
[47] H. Kaur, S. Singh, B. Pal, Applied Surface Science Effect of plasmonic metal (Cu, Ag, and Au) loading over the physicochemical and photocatalytic properties of Mg-Al LDH towards degradation of tetracycline under LED light, Appl. Surf. Sci. 609 (2023), 155455, https://doi.org/10.1016/j.apsusc.2022.155455.